Appl. Phys. B 70, 57–63 (2000) / Digital Object Identifier (DOI) 10.1007/s003409900084

Applied Physics B
Lasers
and Optics

Normal mode expansion method for laser-generated ultrasonic Lamb waves in orthotropic thin plates

J.C. Cheng, T.H. Wang, S.Y. Zhang

State Key Laboratory of Modern Acoustics and Institute of Acoustics, Nanjing University, Nanjing 210093, P.R. China
(E-mail: paslab@nju.edu.cn)

Received: 18 November 1998/Revised version: 19 March 1999/Published online: 29 July 1999

Abstract. A quantitative theory for modeling the laser-generated transient ultrasonic Lamb waves, which propagates along arbitrary directions in orthotropic plates, is presented by employing an expansion method of generalized Lamb wave modes. The displacement field is expressed by a summation of the symmetric and antisymmetric modes in the surface stress-free orthotropic plate, and therefore the theory is particularly appropriate for waveform analyses of Lamb waves in thin plates because one needs only to evaluate several lower modes. The transient waveforms excited by the thermoelastic expansion and the oil-coating evaporation are analyzed for a transversely isotropic thin plate. The results show that the theory provides a quantitative analysis to characterize anisotropic elastic stiffness properties of orthotropic plates by laser-generated Lamb wave detection.

PACS: 43.35.+d; 81.60.Hv; 81.70.Dw

The technique of laser-generated Lamb waves has potential applications to non-contact and nondestructive evaluation and characterization of the sheet materials in industry. It was demonstrated that the thickness and moduli of isotropic thin plates could be measured experimentally without any prior knowledge of the acoustic properties [1, 2]. In determining the plate thickness and moduli it was assumed that the observed waveform was composed of the lowest order symmetric and antisymmetric Lamb modes, due to existence of a cut-off frequency. On the theoretical front, Spicer et al. [3] presented a theoretical formulation for laser–ultrasonic wave generation in an isotropic thin plate by using the numerical inversion of the Hankel–Laplace transform solution to the time-dependent thermal diffusion problem in the hyperbolic form. The effectiveness of this formulation was shown in extracting plate thickness and modulus values by direct comparison of theory with experimental waveforms. Dubois et al. [4] developed a model of the thermoelastic excitation of ultrasound in an orthotropic thick plate based on the temporal Laplace and spatial two-dimensional Fourier transforms for materials having orthotropic symmetry. However, all these theoretical works involved an inverse Laplace integral, which is usually evaluated by the calculus of residues. The evaluation of the inverse Laplace integral in the first approach involves the understanding of the intricate behavior of dispersion relations for real as well as complex wavenumbers, and its physical sense is hard to understand [5].

Another approach, called the normal mode expansion method, has been proposed by Cheng et al. [6] for modeling the thermoelastic generation process of elastic waveforms in an isotropic plate. Cheng and Berthelot [7] have extended this method to Lamb wave propagation along two principal directions in an orthotropic plate. In the principal directions of the orthotropic material, there exist three types of free-plate modes; namely, the pure shear horizontal, dilatational, and flexural modes. The shear horizontal mode polarized parallel to the plate surface is not coupled to the dilatational and flexural modes, which simplifies greatly the Lamb wave motion. However, only seven of the nine independent elastic coefficients of the orthotropic materials are involved, as analyzed in [7], as the Lamb waves propagate in the principal directions. These seven coefficients are c_{11}, c_{22}, c_{33}, c_{44}, c_{55}, c_{13}, and c_{23} in the principal axis coordinate system. In order to extract the other two elastic coefficients (c_{12} and c_{66}) by fitting comparison of theory with experimental waveforms, we had to consider the Lamb wave propagation in the nonsymmetric directions. The Lamb wave propagation in nonsymmetric directions is more complex than that along the principal directions, because there will no longer be a family of shear horizontal modes independent of the dilational and flexural modes in the nonsymmetric directions. All partial waves are coupled, and the free-plate modes can only be classified as symmetric and antisymmetric modes with respect to the median plane. Therefore, it is necessary to develop the work in [7] to Lamb wave propagation in the nonsymmetric directions.

The interest in an orthotropic plate has been motivated by fiber composite material. For the propagation of elastic waves in composite reinforced with large-diameter fibers, the

dynamic effects of the microstructuring must be considered, if the fiber is large enough to equal a longitudinal acoustic quarter-wavelength in the range of 10 to 20 MHz. However, in most fiber composite systems, the fiber diameter is small enough to permit modeling of the material as a homogeneous, but anisotropic, medium, which retains the symmetry of the composite, but ignores its microstructural nature. For a [0/90] cross-ply composite with a unidirectional lamina, the composite plate is considered usually as an equivalent homogeneous orthotropic material and the characteristics of the elastic waves are studied by using the effective stiffness matrix.

In this paper, a quantitative theory to simulate the laser-generated transient Lamb wave propagating along an arbitrary direction in an orthotropic plate is presented by employing the normal mode expansion of generalized Lamb wave modes. The displacement is simply expanded into both the symmetric and antisymmetric wave modes in the surface stress-free orthotropic plate. All factors, such as spatial and time distributions of the incident laser beam, optical penetration, thermal diffusivity, thickness of the plate, and source–receiver distance, can be taken into account. This method is particularly appropriate for waveform analyses of the transient Lamb wave in the thin-sheet materials since we need only to calculate contributions of the lower few antisymmetric and symmetric modes. The transient Lamb waves, excited by thermoelastic expansion and evaporation of the oil, are analyzed numerically for a transversely isotropic thin plate modeling unidirectional composite materials. The numerical analysis shows that the theory provides a quantitative analysis to characterize anisotropic elastic stiffness properties of the orthotropic thin plates by laser-generated Lamb wave detection.

1 Theory

1.1 Basic equations

We consider an infinite plate of finite thickness $2h$ of an orthotropic material. The coordinate axes x_1, x_2, and x_3 of the model are chosen as to be parallel with the principal axes x, y, and z of the material, with z being the optical axis of the incident laser. The $x_3 = \pm h$ are the lower and upper surfaces of the elastic plate, respectively, with $x_3 = 0$ being the midplane of the plate, as shown in Fig. 1. The displacement field vector $\boldsymbol{u} = (u_1, u_2, u_3)$ satisfies

$$\rho \frac{\partial^2 u_i}{\partial t^2} = \sum_{j=1}^{3} \frac{\partial \tau_{ij}(\boldsymbol{u})}{\partial x_j} + f_i \,, \quad (i = 1, 2, \text{ and } 3) \tag{1a}$$

with the boundary conditions at surfaces $x_3 = \pm h$

$$\sum_{j=1}^{3} \tau_{ij}(\boldsymbol{u}) n_j = s_i \,, \quad (i = 1, 2, \text{ and } 3) \tag{1b}$$

where $\boldsymbol{f} = (f_1, f_2, f_3)$ and $\boldsymbol{s} = (s_1, s_2, s_3)$ are the bulk and surface force densities, respectively, induced by the incident laser pulse, ρ is the volume density, $(n_1, n_2, n_3) = (0, 0, \pm 1)$ are the normal vectors at the lower and upper surfaces, respectively, and $\tau_{ij}(\boldsymbol{u})(i, j = 1, 2, \text{ and } 3)$ is the stress tensor. The

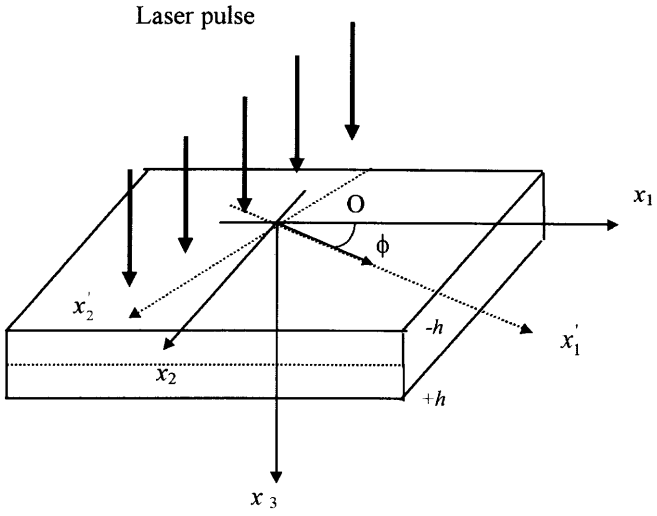

Fig. 1. Geometry of an orthotropic plate, showing Gaussian line oriented in the angle ϕ and Lamb wave propagating along ϕ direction

stress tensor can be expressed by nine non-zero independent elastic constants for an orthotropic material in the symmetric coordinate system

$$\begin{aligned}
\tau_{11} &= c_{11}u_{1,1} + c_{12}u_{2,2} + c_{13}u_{3,3} \,, \\
\tau_{22} &= c_{12}u_{1,1} + c_{22}u_{2,2} + c_{23}u_{3,3} \,, \\
\tau_{33} &= c_{13}u_{1,1} + c_{23}u_{2,2} + c_{33}u_{3,3} \,, \\
\tau_{23} &= c_{44}(u_{2,3} + u_{3,2}) \,, \\
\tau_{13} &= c_{55}(u_{1,3} + u_{3,1}) \,, \\
\tau_{12} &= c_{66}(u_{2,1} + u_{1,2}) \,,
\end{aligned}$$

By the two-dimensional Fourier transform for variables x_1 and x_2

$$u_i(x_1, x_2, x_3, t) = \frac{1}{2\pi} \int_{-\infty}^{\infty} \tilde{u}_i(k_1, k_2, x_3, t) \times \exp[\mathrm{i}(k_1 x_1 + k_2 x_2)] \,\mathrm{d}k_1 \,\mathrm{d}k_2 \,, \tag{2}$$

Equations (1a) and (1b) are reduced to forms of the matrix operators

$$\rho \frac{\partial^2 \tilde{\boldsymbol{u}}}{\partial t^2} = \boldsymbol{a}(\tilde{\boldsymbol{u}}) + \tilde{\boldsymbol{f}} \,, \tag{3a}$$

$$\boldsymbol{b}(\boldsymbol{u}) = \tilde{\boldsymbol{s}} \,, \quad \text{at} \quad x_3 = \pm h \,, \tag{3b}$$

where $\tilde{\boldsymbol{u}} = (\tilde{u}_1, \tilde{u}_2, \tilde{u}_3)^t$ is the displacement column vector, $\tilde{\boldsymbol{f}} = (\tilde{f}_1, \tilde{f}_2, \tilde{f}_3)^t$ and $\tilde{\boldsymbol{s}} = (\tilde{s}_1, \tilde{s}_2, \tilde{s}_3)^t$ are the body and surface force column vectors, respectively, the superscript t represents the transpose, and the elements a_{ij} and b_{ij} of the 3×3

matrix operators $\boldsymbol{a} = (a_{ij})$ and $\boldsymbol{b} = (b_{ij})$ are follows

$$
\begin{aligned}
a_{11} &= -(c_{11}k_1^2 + c_{66}k_2^2) + c_{55}\frac{\partial^2}{\partial x_3^2}\ ;\\
a_{12} &= a_{21} = -(c_{12} + c_{66})k_1k_2\ ,\\
a_{22} &= -(c_{66}k_1^2 + c_{22}k_2^2) + c_{44}\frac{\partial^2}{\partial x_3^2}\ ;\\
a_{23} &= a_{32} = \mathrm{i}(c_{23} + c_{44})k_2\frac{\partial}{\partial x_3}\ ,\\
a_{33} &= -(c_{55}k_1^2 + c_{44}k_2^2) + c_{33}\frac{\partial^2}{\partial x_3^2}\ ;\\
a_{13} &= a_{31} = \mathrm{i}(c_{13} + c_{55})k_1\frac{\partial}{\partial x_3}\ ,
\end{aligned}
$$

and

$$
\begin{aligned}
&b_{11} = c_{55}\frac{\partial}{\partial x_3}\ ;\ b_{12} = 0\ ;\ b_{13} = \mathrm{i}c_{55}k_1\ ,\\
&b_{21} = 0\ ;\ b_{22} = c_{44}\frac{\partial}{\partial x_3}\ ;\ b_{23} = \mathrm{i}c_{44}k_2\ ,\\
&b_{31} = \mathrm{i}c_{31}k_1\ ;\ b_{32} = \mathrm{i}c_{32}k_2\ ;\ b_{33} = c_{33}\frac{\partial}{\partial x_3}\ .
\end{aligned}
$$

1.2 Expansion in normal modes

Usually, (3a) is solved by employing temporal Laplace transformation [3, 4]. However, this technique requires a numerical inverse transform integral evaluated by the calculus of residues, which in the first approach involves the understanding of the intricate behavior of dispersion relations for real and complex wave numbers. Here we employ the method of expansion in normal modes to solve this equation. We define an eigenfunction series $\{\boldsymbol{w}_m, \omega_m, m = 1, 2, 3, \cdots\}$ by the eigenvalue problem of the operator $\boldsymbol{a}$ under the boundary operator $\boldsymbol{b}$

$$
\boldsymbol{a}[\boldsymbol{w}_m] = -\rho\omega_m^2\boldsymbol{w}_m\ , \quad -h < x_3 < +h\ , \tag{4a}
$$

$$
\boldsymbol{b}[\boldsymbol{w}_m] = 0\ , \quad x_3 = \pm h\ , \tag{4b}
$$

where ω_m is the eigenfrequency corresponding to the eigenmode $\boldsymbol{w}_m = [w_{1m}, w_{2m}, w_{3m}]^t$. Because the operator $\boldsymbol{a}$ is a self-adjoint operator under the boundary operator $\boldsymbol{b}$, the eigen-function series $\{\boldsymbol{w}_m\}$ forms an orthogonal set with the weighting function ρ [8],

$$
\int_{-h}^{+h}\rho\boldsymbol{w}_n\boldsymbol{w}_m^{*t}\,\mathrm{d}x_3 = \delta_{mn}\ . \tag{4c}
$$

On the other hand, it has been proven that $\{\boldsymbol{w}_m\}$ is also a complete function series [8], so that the displacement column vector $\tilde{\boldsymbol{u}}$ can be expanded by the generalized Fourier series

$$
\tilde{\boldsymbol{u}}(k_1, k_2, x_3, t) = \sum_m \xi_m(k_1, k_2, \omega_m, t)\boldsymbol{w}_m(k_1, k_2, \omega_m, x_3)\ , \tag{5a}
$$

where $\xi_m(t)$ are the generalized Fourier coefficients

$$
\xi_m = \frac{1}{\omega_m}\int_0^t \sin\omega_m(t-\tau)\left[\tilde{\boldsymbol{s}}\ \boldsymbol{w}_m^{*t}\big|_{x_3=\pm h} + \int_\nu \tilde{\boldsymbol{f}}\boldsymbol{w}_m^{*t}\,\mathrm{d}\nu\right]\mathrm{d}\tau\ , \tag{5b}
$$

where ν represent the body of the plate and the superscript "*" represents complex conjugation.

1.3 Lamb wave modes

In fact, (4a) and (4b) mean that the eigen-functions of the operator $\boldsymbol{a}$ are the generalized Lamb wave modes and the relations between ω_m and (k_1, k_2) are dispersion equations of the Lamb wave modes. The eigenfunctions can be classified as antisymmetric and symmetric modes with respect to the median plane ($x_3 = 0$) [9],

$$
\begin{aligned}
w_{jm}^a &= i\sum_{l=p,q,r}\chi_{jl}\lambda_l e_l\sin\lambda_l x_3\ , \quad j = 1 \text{ and } 2\ ,\\
w_{3m}^a &= \sum_{l=p,q,r} e_l\cos\lambda_l x_3\ ,
\end{aligned} \tag{6a}
$$

for antisymmetric modes and

$$
\begin{aligned}
w_{jm}^s &= -i\sum_{l=p,q,r}\chi_{jl}\lambda_l f_l\cos\lambda_l x_3\ , \quad j = 1 \text{ and } 2\ ,\\
w_{3m}^s &= \sum_{l=p,q,r} f_l\sin\lambda_l x_3\ ,
\end{aligned} \tag{6b}
$$

for symmetric modes. The generalized Rayleigh–Lamb equations for determining the relations between eigen-frequency ω_m and the wavenumbers (k_1 and k_2) can be obtained by combining (6a) and (6b) with (4b)

$$
\det[t_{ij}(\omega_m, k_1, k_2)] = 0\ , \tag{7}
$$

with the elements of 3×3 matrix $\boldsymbol{t} = [t_{ij}]$ ($l = p$, q, and r)

$$
\begin{aligned}
t_{jl} &= (\lambda_l^2\chi_{jl} + k_j)\ , \quad j = 1 \text{ and } 2\ ,\\
t_{3l} &= (c_{13}k_l\chi_{1l} + c_{23}k_2\chi_{2l} + c_{33})\lambda_l[\tan(\lambda_l h)]^{\pm 1}\ .
\end{aligned}
$$

Here the "+1" and "−1" in the element t_{3l} correspond to antisymmetric and symmetric modes, respectively. The parameters in (6a) and (6b) are discussed as follows:

(a) The partial wave numbers λ_l ($l = p$, q, and r) are the roots of the determinant equation

$$
\det[g_{ij}(\lambda)] = 0\ . \tag{8}
$$

This equation is deduced by substituting the partial waves $\nu_{jm} = \nu_{jm}^0\exp(\mathrm{i}\lambda x_3)$ ($j = 1$, 2, and 3) into (4a). The elements of 3×3 symmetric matrix $\boldsymbol{g}(\lambda) = [g_{ij}(\lambda)]$ are

$$
\begin{aligned}
&g_{11}(\lambda) = (\rho\omega_m^2 - a_{11}) - c_{55}\lambda^2\ ;\ g_{12}(\lambda) = g_{21}(\lambda) = -a_{12}\ ,\\
&g_{22}(\lambda) = (\rho\omega_m^2 - a_{22}) - c_{44}\lambda^2\ ;\ g_{13}(\lambda) = g_{31}(\lambda) = -a_{13}\lambda\ ,\\
&g_{33}(\lambda) = (\rho\omega_m^2 - a_{33}) - c_{33}\lambda^2\ ;\ g_{23}(\lambda) = g_{32}(\lambda) = -a_{23}\lambda\ ,
\end{aligned}
$$

(b) The coefficients χ_{1l} and χ_{2l} are the partial wave amplitudes, defined by

$$\chi_{1l} = (a_{13}g_{22} + a_{12}a_{23})/(g_{11}g_{22} - a_{12}^2) \,, \tag{9a}$$

$$\chi_{2l} = (a_{23}g_{11} + a_{12}a_{13})/(g_{11}g_{22} - a_{12}^2) \,. \tag{9b}$$

(c) The amplitudes e_l and f_l ($l = p$ and q) depend on e_r and f_r by following equations

$$\sum_{l=p,q} (t_{jl} \cos \lambda_l h) e_l = -e_r t_{jr} \cos \lambda_r h \,, \quad (j = 1 \text{ and } 2) \tag{10a}$$

$$\sum_{l=p,q} (t_{jl} \sin \lambda_l h) f_l = -f_r t_{jr} \sin \lambda_r h \,, \quad (j = 1 \text{ and } 2) \tag{10b}$$

The e_r or f_r is determined by the normalized condition

$$\int_{-h}^{h} \rho \boldsymbol{w}_m^{a,s} (\boldsymbol{w}_m^{a,s})^{*t} \, \mathrm{d}x_3 = 1 \,. \tag{11}$$

Finally, one can obtain a normalized eigenfunction series $\{\boldsymbol{w}_m^{a,s}\}$ for symmetric and antisymmetric modes.

2 Numerical analyses

For simplicity, a Gaussian line source oriented at the angle ϕ from the x_1 axis, as shown in Fig. 1, is considered in the numerical analyses, and the generalized Lamb wave will propagate along the ϕ direction or the x_1' axis. The spatial distribution $o(x_1, x_2)$ of laser pulse is expressed by

$$o(x_1, x_2) = 1/(2\pi a^2) \exp[-(x_1 \cos\phi + x_2 \sin\phi)^2/a^2] \,, \tag{12}$$

where a is the laser beam radius. The wavenumbers k_1 and k_2 are replaced by $k_1 = k\cos\phi$ and $k_2 = k\sin\phi$, and the displacement field is

$$\boldsymbol{u}(x_1', x_3', t) = \frac{1}{2\pi} \int_o^{\infty} \mathrm{d}k \sum_{m=1}^{\infty} \xi_m(k\cos\phi, k\sin\phi, \omega_m, t) \times \boldsymbol{w}_m(k\cos\phi, k\sin\phi, \omega_m, x_3') \exp(\mathrm{i}kx_1') \,. \tag{13a}$$

It is easy to obtain the surface normal velocity from (13a)

$$v_3(d, t) = \frac{\mathrm{d}u_3(d, -h, t)}{\mathrm{d}t} \,, \tag{13b}$$

where d is the source–receiver distance.

For a transversely isotropic plate, the $(x_2 - x_3)$ plane is isotropic so that there are only five independent stiffness constants. In the numerical simulations, the five elastic constants are $c_{11} = 155.44\,\mathrm{GPa}$, $c_{22} = 15.9\,\mathrm{GPa}$, $c_{55} = 6.08\,\mathrm{GPa}$, $c_{12} = 9.10\,\mathrm{GPa}$, and $c_{23} = 8.14\,\mathrm{GPa}$. The density and the half of thickness are $\rho = 2.5\,\mathrm{g/cm^3}$ and $h = 0.15\,\mathrm{mm}$, respectively. The dispersion curves of each mode can be obtained by solving (7). Figure 2 depicts dispersion curves of two antisymmetric and symmetric modes along two propagating directions of the Lamb wave modes: $\phi = 30°$ and 60°. In Fig. 2, the a_1 and s_0 are two coupled shear horizontal modes, which is different from the isotropic plate [6, 10].

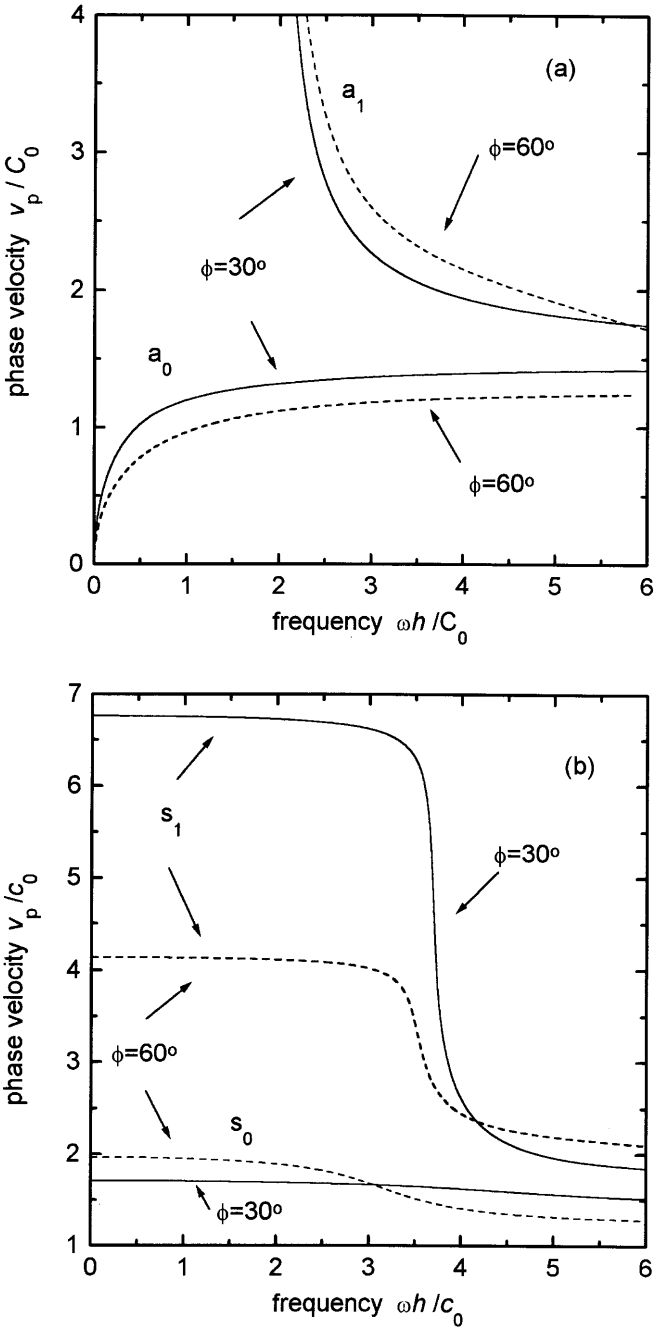

Fig. 2a,b. Dispersion curves of two antisymmetric (**a**) and two symmetric (**b**) modes for different propagating directions $\phi = 30°$ and 60°

2.1 Thermoelastic excitation

The bulk and surface forces $\boldsymbol{f}$ and $\boldsymbol{s}$ depend on not only the energy intensity of the laser pulse, but also the experimental condition. In the thermoelastic regime, a localized temperature variation ϑ in the sample induced by absorption of laser energy results in a localized thermal expansion, which, in turn, generates a transient displacement field $\boldsymbol{u}$. The thermal stress tensor τ_{ij}' is expressed as [11]

$$\tau_{ij}' = \tau_{ij}(\boldsymbol{u}) + \beta_{ij}\vartheta \,, \tag{14a}$$

where β_{ij} is the stiffness expansion tensor. In the principal axis coordinate system, only three diagonal elements (β_{11}, β_{22}, and β_{13}) are non-zero, which can be expressed by three elements of the thermal expansion tensor a_{ij}:

$$\beta_{ii} = -\sum_{j=1}^{3} c_{ij}\alpha_{jj} \quad (i = 1, 2, \text{ and } 3) \,. \tag{14b}$$

Therefore, the equivalent bulk and surface force densities resulting from the thermal stress are

$$f_i = \sum_{j=1}^{3} \beta_{ij} \frac{\partial \vartheta}{\partial x_j} \,, \quad (i = 1, 2, \text{ and } 3) \tag{15a}$$

$$s_i = -\sum_{j=1}^{3} \beta_{ij} n_j \vartheta \,, \quad (i = 1, 2, \text{ and } 3) \,. \tag{15b}$$

The temperature distribution $\vartheta(x_1, x_2, x_3, t)$ satisfies the thermal diffusion equation

$$\rho c \frac{\partial \vartheta}{\partial t} - \sum_{i,j=1}^{3} \kappa_{ij} \frac{\partial^2 \vartheta}{\partial x_i \partial x_j} = q \,, \tag{16a}$$

where c is the specific heat, κ_{ij} is the thermal conductivity tensor, and $q = q(x_1, x_2, x_3, t)$ is the heating source due to absorption of the incident laser pulse, which is expressed by, assuming that absorption of laser energy is isotropic,

$$q = q_0 \beta o(x_1, x_2) \exp[-\beta(x_3 + h)] g(t) \,, \tag{16b}$$

where q_0 is the totally absorbed laser energy, $1/\beta$ is the optical penetration depth, and $g(t)$ is the temporal distribution of laser pulse. The laser pulse, whose duration is on the order of nano-seconds, is extremely short compared to wave propagation times, which is on the order of microseconds, and can be adequately represented by assuming $g(t)$ as Dirac's delta function $\delta(t)$ [12]. Typically, β are on the order of 10^5 to

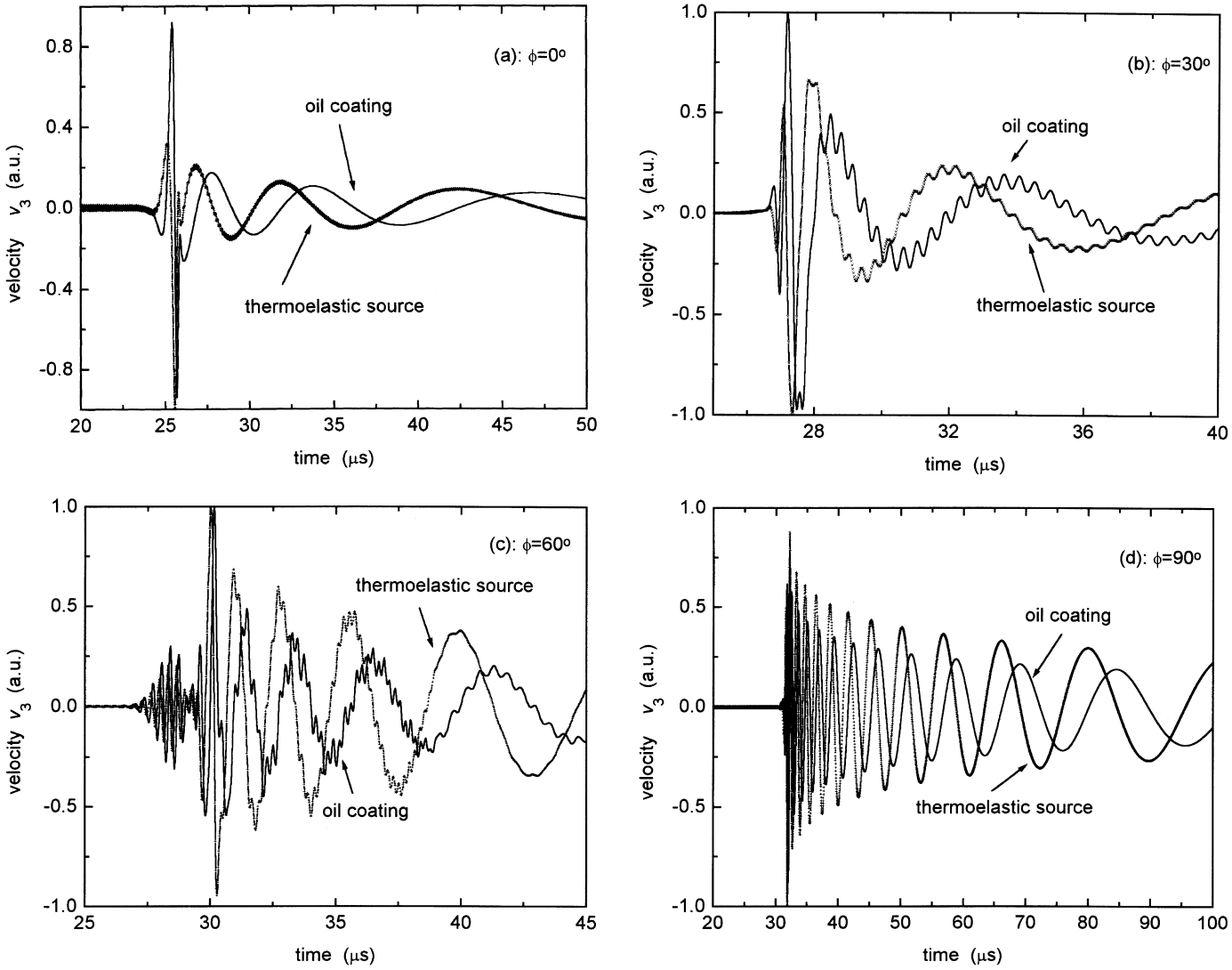

Fig. 3a–d. Surface normal velocity v_3 of the far-field transient Lamb waveforms propagating along directions $\phi = 0°$, 30°, 60°, and 90° by the thermoelastic excitation and the oil-coating evaporation generation with the source–receiver distance $d = 4.0$ cm in (**a**), (**b**), (**c**), and (**d**), respectively

$10^6\ \mathrm{cm}^{-1}$ for metals and some opaque solids, therefore an assumption of surface absorption (i.e., zero absorption depth) is reasonable. The temporal temperature reaches its maximum rapidly on the order of nanoseconds for the laser pulse $\delta(t)$, and then decays slowly. This temporal characteristic can be approximated by the unit step function $H(t)$ in the scale of microseconds, which means that the second term in (16a), representing the thermal diffusivity, is negligible for small thermal conductivity [12]. In fact, the time dependence of force sources induced by thermoelastic expansion can be approximately by $H(t)$ to predict the observed waveforms [13].

Therefore, for simplicity, three approximations are assumed in numerical analyses: (a) the laser pulse shape is $\delta(t)$; (b) the absorption depth is zero $1/\beta \approx 0$; and (c) the thermal diffusion is neglected. In these conditions, the solution of (16a) is simply

$$\vartheta = \frac{q_0}{\rho c} o(x_1, x_2)\delta(x_3 + h)H(t)\ . \tag{17}$$

Then, one can obtain the surface normal velocity by combining (15a) and (15b) with (17). In numerical analyses, the thermal expansion coefficients $\alpha_{11} = 5.0 \times 10^{-6}\,/\mathrm{K}$, $\alpha_{22} = 1.0 \times 10^{-6}\,/\mathrm{K}$ and $\alpha_{33} = 1.0 \times 10^{-6}\,/\mathrm{K}$, and the width of Gaussian beam radium is $a = 0.20\,\mathrm{mm}$. The transient Lamb waveforms excited by the thermoelastic expansion are shown in Fig. 3 for propagating along different directions $\phi = 0°$, 30°, 60°, and 90°.

2.2 Oil-coating evaporation

In experiments, a thin coating of oil at the generation spot is used to increase the acoustic generation efficiency from the laser pulse. In this case, both the thermoelastic expansion and evaporation of the oil will generate the force sources at the same time. But evaporation of the oil become dominant sources [13, 14]. The generation mechanism of the force sources by evaporation of the oil is that momentum is transferred from the evaporating particles to the solid surface. The researches by Hutchins et al. [13, 14] showed that the evaporating force source is dominated by a normal force monopole with $\delta(t)$ time dependence. This implies that the recoil force from ablation of the oil depresses the surface, and then rapidly returns to its equilibrium position. Therefore, the bulk force density $\boldsymbol{f} = 0$ and the surface force density $\boldsymbol{s} = (0, 0, s_3)$ are approximately proportional to the incident laser pulse

$$s_3(x_1, x_2, t) = \eta o(x_1, x_2)\delta(t)\ , \tag{18}$$

where η is the efficiency constant. Substituting this surface force source into (5b) yields

$$\xi_m^{a,s} = -\eta\tilde{o}(k_1, k_2)\frac{\sin\omega_m t}{\omega_m}\ w_{3m}^{a,s}\big|_{x_3=-h}\ . \tag{19}$$

The transient Lamb waveforms excited by the oil-coating evaporation are shown also in Fig. 3 for propagating along different directions $\phi = 0°$, 30°, 60°, and 90°.

In an orthotropic plate, each Lamb mode has a cut-off frequency, except for zero-order antisymmetric mode a_0 and two lower symmetric modes s_0 and s_1. The cut-off frequency f_c depends on the propagating direction and the plate thickness. For antisymmetric mode a_3, $f_c \approx 5.94C_0/(2\pi h) \approx 6.3\,\mathrm{MHz}$ ($C_0 = 10^3\,\mathrm{m/s}$ and $h = 0.15\,\mathrm{mm}$) in the numerical analyses for propagating direction $\phi = 30°$. This is greater than the maximum frequency component $f_{\max} \approx C_0/a \approx 5.0\,\mathrm{MHz}$ generated by the thermoelastic expansion and the oil-coating evaporation. Therefore, we need only to consider six modes (a_0, a_1, a_2) and (s_0, s_1, s_2) to calculate the far-field transient Lamb waveforms for a thin plate. In fact, the contributions of the higher modes to the surface normal velocity v_3 are very small and can be ignored because the plate is thin ($h = 0.15\,\mathrm{mm}$) in the numerical calculations. In Fig. 3, only the modes a_0 and a_1 are calculated because the contribution to v_3 from the symmetric modes is much less than that from the a_0 and a_1.

Figure 3 shows the typical transient Lamb waveforms, which consist of the first arrival of the higher frequencies and the later lower-frequency signal of the lowest antisymmetric a_0 mode. The higher-frequency oscillations at the waveforms in Figs. 3b and 3c come from the contribution of the mode a_1. Figure 3 indicates also that the transient Lamb waveforms are sensitive to anisotropic properties of the materials by comparing the waveforms at different directions.

The epicenter waveforms have totally different temporal characteristics for thermoelastic and evaporting generations in bulk materials [13]. But Fig. 3 shows that the transient Lamb waveforms induced by the former are similar to the waveforms generated by the latter, although the time dependence of force source in two cases are completely different. The similarity indicates that the a_0 and a_1 modes can be excited by both the force sources. This implies that excitation of a_0 and a_1 modes depends weakly on the temporal distribution of the force source for thin plate.

On the other hand, Figs. 3b and 3c show apparently the contribution of coupled shear horizontal mode a_1. In contrast with the results obtained in [7], the shear horizontal modes are not coupled to the surface normal velocity as the Lamb waves propagate along two principal directions in an orthotropic plate, as shown in Figs. 3a and 3d.

3 Conclusion

A theory to simulate excitation of transient Lamb wave propagating along arbitrary directions in orthotropic plates is presented by employing the normal mode expansion method of the Lamb wave modes. The displacement field vector is expressed by a summation of the symmetric and antisymmetric modes in the surface stress-free orthotropic plate. The theory is particularly appropriate for waveform analyses of Lamb wave in thin plates because one needs only to evaluate the lower several modes. The numerical analyses indicate that the method will provide a useful technique to characterize anisotropic properties of orthotropic thin plates. However, it is available to consider not only the higher frequency components of the lowest Lamb wave modes, but also the higher-order Lamb wave modes for thicker plates in the numerical analyses. The further investigations are in progress.

Acknowledgements. This work is supported by the National Science Foundation of China under Grant No. 19574024 and the Natural Science Foundation of Jiangsu Province under Grant No. BK97031.

References

1. R.J. Dewhurst, C. Edwards, A.D.W. McKie, S.B. Palmer: Appl. Phys. Lett. **51**, 1066 (1987)
2. L. Noui, R.J. Dewhurst: Appl. Phys. Lett. **57**, 551 (1990)
3. J.B. Spicer, A.D.W. McKie, J.W. Wagner: Appl. Phys. Lett. **57**, 1882 (1990)
4. M. Dubois, F. Enguehard, L. Bertrand, M. Choquet, J.P. Monchalin: Appl. Phys. Lett. **64**, 554 (1994)
5. R.L. Weaver, Y.H. Pao: J. Appl. Mech. **49**, 821 (1982)
6. J.C. Cheng, S.Y. Zhang, L. Wu: Appl. Phys. A **61**, 311 (1995)
7. J.C. Cheng, Y. Berthelot: J. Phys. D **29**, 1857 (1996)
8. C. Eringen, E.S. Suhubi: *Elastodynamics* (Academic Press, New York 1975) Vol. 2
9. J.C. Cheng, S.Y. Zhang: Rev. Prog. Quant. Non-Destr. Eval. **15**, 253 (1996)
10. L. Wu, J.C. Cheng, S.Y. Zhang: J Phys. D **28**, 957 (1995)
11. W. Nowacki: *Thermoelastivity*, 2nd edn. (Pergamon, Oxford 1986)
12. K.L. Telschow, R.J. Conant: J. Acoust. Soc. Am. **88**, 1497 (1990)
13. D.A. Hutchins, R.J. Dewhurst, S.B. Palmer: Appl. Phys. Lett. **38**, 677 (1981)
14. D.A. Hutchins, R.J. Dewhurst, S.B. Palmer: Ultrasonics 103 (1981)